

Generalized phase diffraction gratings with tailored intensity

Jorge Albero,^{1,*} Ignacio Moreno,¹ Jeffrey A. Davis,² Don M. Cottrell,² and David Sand²

¹Dept. de Ciencia de Materiales, Óptica y Tecnología Electrónica, Universidad Miguel Hernández, 03202 Elche, Spain

²Department of Physics, San Diego State University, San Diego, California 92182-1233, USA

*Corresponding author: j.albero@umh.es

Received June 8, 2012; revised August 29, 2012; accepted September 12, 2012;
posted September 13, 2012 (Doc. ID 170276); published October 5, 2012

We report the generation of continuous phase masks designed to generate a set of target diffraction orders with defined relative intensity weights. We apply a previously reported analytic calculation that requires resolving a single equation with a set of parameters defining the target diffraction orders. Then the same phase map is extended to other phase patterns such as vortex generating/sensing gratings. Results are demonstrated experimentally with a parallel-aligned spatial light modulator. © 2012 Optical Society of America
OCIS codes: 230.3720, 230.6120, 050.1970.

Diffraction optical elements (DOEs) find a wide field of applications in beam splitting. For instance, laser processing and microscopy profit from beam splitting for simultaneous processing with a multispot pattern [1–3]. Many theoretical studies have proven that DOEs are suitable to separate light into a number N of beams with high efficiency, including binary phase Dammann gratings [4] or continuous phase profiles [5,6]. Different types of iterative algorithms can be used to calculate phase holograms with desired optical responses, where the inverse Fourier transform [7] is among the most used. These iterative algorithms have also been applied to generate arrays of equally intense diffraction orders [8]. However, optimal efficient diffraction grating fan-out elements can be analytically solved using a single equation with a limited set of parameters. For instance, Gori *et al.* solved the optimal triplicator in [9], and Romero and Dickey further extended the technique to an arbitrary number of target diffraction orders in [10]. However, one can barely find experimental realizations of this last kind of gratings in the literature due to the difficulties in reproducing the derived continuous phase profiles [11]. Spatial light modulators (SLMs) have been recently demonstrated to be useful to generate equi-intense beams with this method [12].

In general the fan-out elements are designed to generate a set of target diffraction orders, all with equal energy. However, tailoring the energies can find applications when the pattern on each order is different. An example is the vortex generating/sensing grating [13], obtained by the addition of the regular blazed grating and the helical phase. In previous studies, we showed that the binarization of such phase profile generates a set of diffraction orders. Each of them shows a vortex beam with a topological charge equal to the product of the encoded order of the helical phase and the diffraction order index. A regular phase binarization was applied in [14], while a binary version based on Dammann gratings was applied in [15], this last showing equal energies for all target orders. However, as the topological charge of the vortex beam increases, the diameter of the generated doughnut diffraction order also increases. Therefore, a diffraction grating with equal energy in the various orders does not generate equally intense doughnut beams because

their diameters are different and the energy is distributed across a wider area.

In this Letter, we produce a variation on previous approaches [10] for producing high efficiency grating beam splitters, where the energies of the output beams have a predefined nonuniform distribution. As an example, we use this method to produce a vortex-generating grating where the intensities of the doughnut beams at each different orders are all equal, in opposition to what happens in those reported in [13–15].

The grating phase profile is obtained from the theory of optimal beam splitting proposed by Prongué *et al.* [5] and further extended by Romero and Dickey [10]. The method consists of determining a phase-only function,

$$\exp[i\varphi(x)], \quad (1)$$

that generates a set of target diffraction orders with a maximum overall efficiency η (defined as the sum of the normalized energies of all these target orders). In addition, the energy of each order can be independently selected. Let a_k be the k th Fourier coefficient of (1), i.e.,

$$a_k = \frac{1}{2\pi} \int_{-\pi}^{\pi} \exp[i\varphi(x)] \exp[-ikx] dx, \quad (2)$$

where one-dimensional gratings with 2π period are considered, and where x denotes the spatial coordinate. The optimal phase function can be obtained as [9]

$$\exp[i\varphi(x)] = \frac{s(x)}{|s(x)|}, \quad (3)$$

where

$$s(x) = \sum_{k=-m}^m \mu_k \exp[i\alpha_k] \exp[ikx]. \quad (4)$$

Here α_k and μ_k are parameters representing the phase and amplitude of the diffraction orders to be symmetric with respect to the zero orders, as $k = 0, \pm 1, \dots, \pm m$. The overall efficiency is defined as:

$$\eta = \frac{\sum_{k=-m}^m |a_k|^2}{\sum_{k=-\infty}^{\infty} |a_k|^2}. \quad (5)$$

Following [10], first the phases α_k are computationally determined in order to achieve the highest η possible. Second, the amplitudes μ_k are included in the optimization to distribute the energy among the target-diffracted orders. The optimization of Eqs. (2)–(5) can be performed with advanced numerical tools. We used the solver routine in Microsoft Excel, which employs a generalized reduced gradient algorithm [16]. The result is a phase-only mapping that can be applied to transform a linear phase blazed grating profile $\phi(x) = 2\pi x/p$ onto the optimal phase profile $\varphi(x)$, as shown in Fig. 1. Here p denotes the period of the grating. The same type of phase mapping can be applied to produce generalized optimal gratings, as shown later.

This theory, detailed in [10], has been devoted to generate diffracted orders with the same energy. Here, we experimentally demonstrate that the same considerations can be useful to obtain an uneven distribution of the output energies. The latter is especially relevant when the diffracted orders carry a pattern, such as the above-mentioned vortex generating diffraction gratings.

On the numerical computation, the intensity of each order $I_k = |a_k|^2$ can be properly set in order to distribute the energies of the various diffracted orders as desired. The calculated phase profile $\exp[i\varphi(x)]$ is experimentally tested with a transmissive parallel-aligned liquid crystal (LC) SLM manufactured by Seiko–Epson, with 640×480 pixels and pixel spacing of $\Delta = 42 \mu\text{m}$ [17]. The SLM is illuminated with an Ar ion laser operating at 514 nm, producing a phase-only modulation exceeding 2π radians. The beam is expanded with a spatial filter, collimated with a lens and linearly polarized parallel to the LC director axis. After passing through the SLM, the beam is focused by a lens to a WinCamD camera.

To show the ability to control the intensity of the diffraction orders, we use a grating beam splitter designed to generate $N = 7$ orders (0, ± 1 , ± 2 and ± 3). Let us first consider that all diffracted orders have the same energies. Figure 2(a) shows the experimental images and their associated intensity profiles, shown as a side view of a 3D profile. Figure 2(b) shows the grey-level grating encoded on the SLM to obtain this result. Figure 2(c) shows the phase profile within one period. This profile is calculated with Eqs. (3) and (4), where the computationally determined μ_k parameters are $\mu_0 = 1$, $\mu_{\pm 1} = 1.272$, $\mu_{\pm 2} = 1.427$, and $\mu_{\pm 3} = 1.241$, while the computationally determined α parameters are (in radians) $\alpha_k = 0$, $\alpha_{\pm 1} = -1.191$, $\alpha_{\pm 2} = 1.764$, and $\alpha_{\pm 3} = 0.670$. The theoretical total efficiency of this grating is $\eta = 0.968$, where the

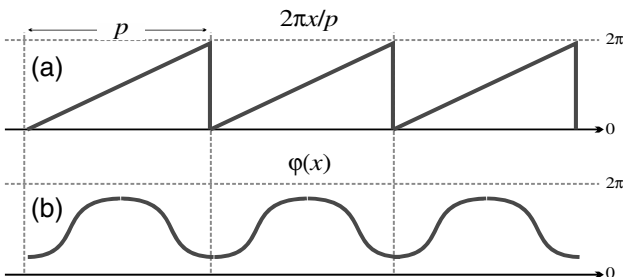


Fig. 1. Phase mapping to generate the optimal phase grating $\varphi(x)$ from a linear blazed grating ($\phi(x) = 2\pi x/p$) of the same period p .

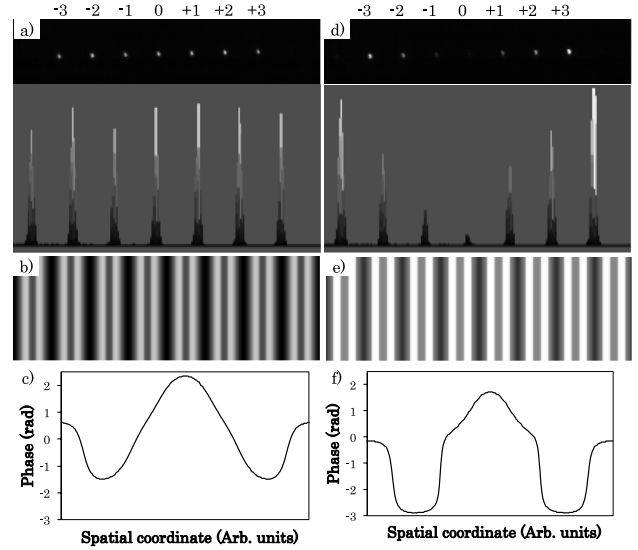


Fig. 2. Experimental $N = 7$ beam splitter (a) equi-energy spots and their profile, (b) detail of the phase grating encoded on the SLM to obtain Fig. 2(a) (c) phase profile corresponding to one period of Fig. 2(b), (d) spots with different energies and their profile, (e) detail of the phase grating encoded on the SLM to obtain the results in Fig. 2(d), and (f) phase profile corresponding to one period in Fig. 2(e).

intensity of each of the seven diffraction orders is equal to 0.139. The experimental grating is reproduced with a period of $p = 64$ pixels. The result in Fig. 2(a) shows the generation of all seven orders with very similar intensities. Note that the intensity profiles are captured from—dynamic imaging instead of postprocessing. Therefore, laser fluctuations are responsible for the instantaneous (slight but nonetheless noticeable) intensity differences.

Figure 2(d) shows the corresponding result when intensity compensation is introduced. In this case we set the energies of the ± 1 st orders as the reference, $I_{\pm 1} = 1$ arbitrary units, and the energies of the ± 2 nd and ± 3 rd orders are selected to be $I_{\pm 2} = \sqrt{2}I_{\pm 1}$ and $I_{\pm 3} = \sqrt{3}I_{\pm 1}$, respectively. The zero order energy is selected to be $I_0 = 0.05I_{\pm 1}$. As in the previous case, Fig. 2(e) shows the gray-level grating encoded on the SLM and, similarly, Fig. 2(f) shows one period of the phase grating. In this case, computationally determined μ_k parameters are $\mu_0 = 1$, $\mu_{\pm 1} = -1.399$, $\mu_{\pm 2} = 0.327$, and $\mu_{\pm 3} = -0.053$, while the computationally determined α_k parameters are $\alpha_0 = 0$, $\alpha_{\pm 1} = 6.831$, $\alpha_{\pm 2} = 11.646$, and $\alpha_{\pm 3} = 12.038$ radians. The overall theoretical efficiency in the seven target diffraction orders is now $\eta = 0.862$, where the relative efficiencies of the various orders are $\eta_0 = 0.005$, $\eta_{\pm 1} = 0.103$, $\eta_{\pm 2} = 0.146$, and $\eta_{\pm 3} = 0.179$, in accordance with the selected ratios. The experimental result in Fig. 2(d) verifies the selected generation of the seven target diffraction orders with their energy ratios.

A vortex grating is formed from a blazed grating by adding a circular helical phase to the linear phase grating [13]. The diffracted order will then show, in the Fourier plane, the typical beam with a singularity at the center, i.e., a ring of light. If the grating is modified to produce N fan-out beams, at the k th diffraction order, the topological charge of the vortex is k times the order ℓ of the helical phase (defined as the number of phase cycles

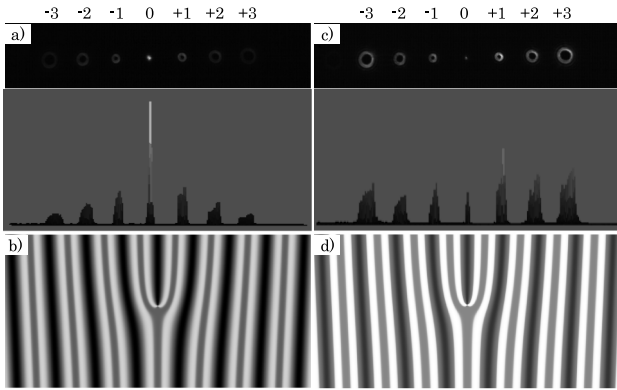


Fig. 3. Experimental $N = 7$ vortex grating (a) equal energy distribution among diffraction orders and their profile, (b) phase grating encoded on the SLM to obtain Fig. 3(a), (c) compensated energy for equi-intense vortices and their profile, and (d) phase grating encoded on the SLM to obtain Fig. 3(c).

$0 - 2\pi$ in a complete 360° cycle). The radius r of each ring is related to the topological charge of the vortex as [18], i.e.,

$$r \propto \sqrt{|k\ell|}. \quad (6)$$

Thus, if the helical phase $\ell = 1$ is added to the linear phase, and the phase transformation given by Eq. (3) to generate the $N = 7$ grating is applied to the resulting phase mask, seven vortex beams will be created with topological charges $0, \pm 1, \pm 2$ and ± 3 .

If these seven orders are selected to have the same energy, the intensity ratio decreases as the order k increases, resulting in a less intense pattern for the higher orders. This is shown in Figs. 3(a) and 3(b), which show the experimental results and their corresponding phase mask. This phase mask is obtained by applying the same phase mapping transformation that was applied in Fig. 2(b)–2(c), to the phase pattern obtained after adding the helical and the linear phases. A detail of the central part of the phase profiles to obtain the vortex grating is shown in Fig. 3(b), illustrating the typical forked grating. The reduction of the intensity of the doughnut beams as the diffraction order increases is clearly visible in the experimental result.

We can, however, force the relative amplitudes to be higher when needed. Therefore, we increased the relative energy of each order by a factor proportional to the radius of each vortex. The values selected for the grating in Fig. 2(e) exactly compensate for the increase in the perimeter $2\pi r$ of the circular diffraction order (for simplicity, we approximate that the energy of the diffraction order is spread onto rings of infinitesimal width). The zeroth order is a special case, since $k = 0$ and there is no actual radius associated with the zero topological charge. For this order we simply evaluated the relative energy required to achieve equivalent intensity,

which corresponds to the value $I_0 = 0.05I_{\pm 1}$ selected in Figs. 2(d)–2(f).

The energy compensation that was applied to the grating in Fig. 2(e) exactly matches the energy of the circular orders generated by the vortex diffraction grating. This is shown in Fig. 3(c), where we reproduce the vortex grating for $N = 7$ with this previously calculated phase mapping transformation. Again, the detail of the central part of the phase mask is shown in Fig. 3(d). Now the results show that the intensity levels for all of the vortices are equalized and the circles at the diffraction orders have all the same visual appearance.

In conclusion, we have experimentally demonstrated with SLMs the realization of phase diffraction gratings with tailored energy at the selected target orders. We have applied it to more generalized patterns like the vortex generating grating, and the energy distribution was adjusted to visualize all circular diffraction orders with equal average intensity, despite the variation of the topological charge in each diffraction order (and subsequently the radius of the beam). We expect that this approach will be useful in a variety of other applications.

I. Moreno and J. Albero acknowledge financial support from Spanish Ministerio de Ciencia e Innovación (ref. FIS2009-13955-C02-02). J. Albero acknowledges financial support from the Spanish Ministerio de Educación through the Programa Nacional de Movilidad de Recursos Humanos, PN I+D+i 2008-2011.

References

1. M. Sakakura, T. Sawano, Y. Shimotsuna, K. Miura, and K. Hirao, *Opt. Express* **18**, 12136 (2010).
2. D. Grier, *Nature* **424**, 810 (2003).
3. M. Montes-Usategui, E. Pleguezuelos, J. Andilla, and E. Martín-Badosa, *Opt. Express* **14**, 2101 (2006).
4. H. Dammann and K. Görtler, *Opt. Commun* **3**, 312 (1971).
5. D. Prongué, H. P. Herzig, R. Dändliker, and M. T. Gale, *Appl. Opt.* **31**, 5706 (1992).
6. J. Bengtsson, *Appl. Opt.* **36**, 8435 (1997).
7. R. W. Gerchberg and W. O. Saxton, *Optik* **35**, 237 (1972).
8. R. Di Leonardo, F. Ianni, and G. Ruocco, *Opt. Express* **15**, 1913 (2007).
9. F. Gori, M. Santarsiero, S. Vicalvi, R. Borghi, G. Cincotti, E. Di Fabrizio, and M. Gentili, *Opt. Commun.* **157**, 13 (1998).
10. L. A. Romero and F. M. Dickey, *Prog. Opt.* **54**, 319 (2010).
11. Y. V. Miklyayev, W. Imgrunt, T. Bizjak, L. Aschke, V. N. Lissotschenko, V. S. Pavelyev, and D. G. Kachalov, *Proc. SPIE* **7640**, 764024 (2010).
12. J. Albero and I. Moreno, *J. Opt.* **14**, 075704 (2012).
13. V. Yu Bazhenov, V. Vashnetsov, and M. S. Soskin, *J. Exp. Theor. Phys. Lett.* **52**, 429 (1990).
14. I. Moreno, J. A. Davis, B. M. L. Pascoguin, M. J. Mitry, and D. M. Cottrell, *Opt. Lett.* **34**, 2927 (2009).
15. I. Moreno, J. A. Davis, D. M. Cottrell, N. Zhang, and X.-C. Yuan, *Opt. Lett.* **35**, 1536 (2010).
16. <http://support.microsoft.com/kb/214115>.
17. J. A. Davis, P. Tsai, D. M. Cottrell, T. Sonehara, and J. Amako, *Opt. Eng.* **38**, 1051 (1999).
18. M. J. Padgett and L. Allen, *Opt. Commun.* **121**, 36 (1995).